CFD Modeling of Gas-Fluidized Beds with a Bimodal Particle Mixture

B. G. M. van Wachem, J. C. Schouten, and C. M. van den Bleek
DelftChemTech, Chemical Reactor Engineering Section, Delft University of Technology, 2628 BL Delft, The Netherlands

R. Krishna
Dept. of Chemical Engineering, University of Amsterdam, 1018 WV Amsterdam, The Netherlands

J. L. Sinclair
School of Chemical Engineering, Purdue University, West Lafayette, IN 47907

A computational fluid dynamics model was developed for gas-solid fluidized beds containing a mixture of two particle species. To calculate stresses of the solid phase, the kinetic theory of granular flow was extended to consider a binary mixture of smooth, nearly elastic, spheres. The developed model was simulated to demonstrate key features of binary mixture fluidization. Bed expansion with a binary mixture of different size particles, but with identical densities, was much higher than that of a system consisting of mono-sized particles of the same mean size as the bimodal mixture. Minimum fluidization velocity for the binary particle system was significantly lowered. The mixing behavior of the binary mixture of particles, characterized by the mixing index, increased with increasing superficial gas velocity. For a binary mixture of particles of larger size with lower density and smaller size with higher density, larger, lighter particles segregated to the top of the fluid bed, while smaller, heavier particles segregated to the bottom. With increasing fluidization velocity, this segregation pattern reversed and ''inversion'' occurred. The drag and gravity force difference between small, heavy particles and large, light particles was dominant at low gas velocities. With an increase in gas velocity, however, the gradients in granular temperature and pressure became dominant terms in the equations for the relative force and thus velocity between two different particle species.

Introduction

It is well known in practice that the particle size distribution (PSD) plays an important role in the behavior of gas-solid mixtures. Many researchers have studied the effect of the PSD on the hydrodynamic behavior of fluidized beds. For instance, De Groot and In Drinkenberg (1967) concluded that the bed expansion of industrial fluidized beds may increase by a factor of two when a large PSD is employed instead of a monodisperse distribution.

Grace and Sun (1991) performed numerous fluidized-bed experiments with a monodisperse, a bimodal, and a wide particle-size/weight distribution of Geldart type A particles. Grace and Sun (1991) studied the influence of ''fines'' on the hydrodynamics in the fluidized bed. They defined fines as particles with a diameter less than approximately 40 μm. They reported that the minimum fluidization velocity was higher with the wide or bimodal PSD vs. the monodisperse PSD with the same mean size. Also, as previously concluded by De Groot (1967), the bed expansion was larger for a wide or bimodal PSD than for a monodisperse PSD. This difference of bed expansion is small around the minimum fluidization ve-

Current address of B. G. M. van Wachem and J. C. Schouten: Laboratory of Chemical Reactor Engineering, Eindhoven University of Technology, 5600 MB Eindhoven, The Netherlands.

locity and increased with increasing superficial gas velocity. Although the experiments of Grace and Sun (1991) were carried out with small particles of Geldart A type, their results present a good qualitative description of the different types of behavior of fluidized beds with a monodisperse PSD and a bimodal PSD.

In a fluidized-bed reactor, the mixing action is produced by the rising of bubbles, whose associated wake and drift leads to the motion of particles. The bubbles in a fluidized bed containing a binary mixture also cause segregation. In fluidized beds containing a binary particle mixture, either by size or density, complete mixing is only achieved under specific hydrodynamic conditions. Wu and Baeyens (1998) experimentally studied the effect of a bimodal PSD on the mixing action in fluidized beds with fairly large particle types, both Geldart B and D type particles. They defined a mixing index M

$$M = \frac{X}{\langle X \rangle} \tag{1}$$

where X is the concentration of larger/heavier particles in the top region of the dense bed, and $\langle X \rangle$ is the average concentration of larger/heavier particles in the entire bed. M equal to 1 corresponds to perfect mixing. Wu and Baeyens (1998) correlated the mixing index to the superficial gas velocity, the bed aspect ratio (H/D_T), the minimum fluidization velocity of the smaller and larger particles, and the particle diameter ratio. The mixing index was small for gas velocities near the minimum fluidization velocity, and increased with gas velocity. The scatter on their correlation was, however, very large.

Rasul et al. (1999) studied the different types of segregation occurring in fluidized beds containing a bimodal PSD, by studying the ''segregation potential'' of fluidized beds containing a bimodal PSD. Specifically, they studied the case of a binary mixture with small, heavy particles and large, lighter particles. At a low fluidization gas velocity, the small, heavy particles were preferentially segregated at the bottom of the fluidized bed, and large, lighter particles were at the top. With increasing gas velocity, ''inversion'' can occur. This means that the small, heavy particles moved preferentially upward in the bed and the light, larger particles moved downward.

The main objective of our work is to simulate the flow behavior of fluidized beds containing a bimodal PSD and to compare this flow behavior with that of fluidized beds containing a monodisperse PSD. The simulation predictions are compared with the experimental data and observations of the authors mentioned above. The details of the physics behind the previous experimental results are elucidated via the simulations.

Governing Equations

The two-fluid model is applied to describe the flow of the dense gas-solid mixture. The continuity equations of the gas phase and the particle mixture phase are

$$\frac{\partial \epsilon_g}{\partial t} + \nabla \cdot (\epsilon_g u_g) = 0 \tag{2}$$

$$\frac{\partial \epsilon_s}{\partial t} + \nabla \cdot (\epsilon_s u_s) = 0 \tag{3}$$

where u_g is the gas-phase velocity and ϵ_g is the gas-phase volume fraction. The momentum balances for the gas phase and the particle mixture follow Jackson (1997)

$$\rho_g \epsilon_g \left[\frac{\partial u_g}{\partial t} + u_g \nabla u_g \right] = \epsilon_g \nabla \cdot \bar{\bar{\tau}}_g - \epsilon_g \nabla P - \beta (u_g - u_s) + \epsilon_g \rho_g g \tag{4}$$

$$\rho_s \epsilon_s \left[\frac{\partial u_s}{\partial t} + u_s \nabla u_s \right] = \epsilon_s \nabla \cdot \bar{\bar{\tau}}_g - \epsilon_s \nabla P + \nabla \cdot \bar{\bar{P}}_s + \beta (u_g - u_s) + \epsilon_s \rho_s g \tag{5}$$

where P is the gas-phase pressure, g is the gravity acceleration, β is the interphase momentum transfer coefficient, $\bar{\bar{\tau}}_g$ is the gas-phase shear stress tensor which is assumed Newtonian, and $\bar{\bar{P}}_s$ is the solids-phase stress tensor with a kinetic and collisional contribution (given by kinetic theory) and also a frictional contribution

$$\bar{\bar{P}}_s = \bar{\bar{P}}_{s,\text{kinetic}} + \bar{\bar{P}}_{s,\text{collision}} + \bar{\bar{P}}_{s,\text{friction}} \tag{6}$$

Pirog (1998) proposed the following modification of the Wen and Yu (1966) equation for the drag force exerting on a particle in the vicinity of other particles

$$\beta_i = \frac{3}{4} f_i(\epsilon_{s,A}, \epsilon_{s,B}) C_D \frac{\epsilon_g \epsilon_{s,i} \rho_s |u_g - u_s|}{d_s} \tag{7}$$

where $f_i(\epsilon_s)$ is the hindered settling velocity function, which is defined as $f_i(\epsilon_{s,A}, \epsilon_{s,B}) = V_i/V_{i,0}$. V_i is the actual settling velocity for the particle in the suspension and $V_{i,0}$ is the settling velocity of an isolated particle. The drag coefficient proposed by Rowe (1961) is employed

$$C_D = \begin{cases} \dfrac{24}{Re_p(1-\epsilon_s)} \left[1 + 0.15 \left\{ (1-\epsilon_s) Re_p \right\}^{0.687} \right] & \text{if } (1-\epsilon_s) Re_p < 1{,}000 \\ 0.44 & \text{if } (1-\epsilon_s) Re_p \geq 1{,}000 \end{cases} \tag{8}$$

In the case of a bimodal particle mixture, $i = A$ or B, and the total interphase momentum transfer coefficient is $\beta = \beta_A + \beta_B$. Pirog (1998) proposed for the settling velocity function

for species i in a bimodal suspension

$$f_i(\epsilon_{s,A},\epsilon_{s,B}) = \prod_{q=A,B}(1-\epsilon_{s,q})^{\alpha_{iq}} \tag{9}$$

where α_{ij} are empirically determined constants in the form of

$$\alpha_{ij} = a_0 + a_1\left(\frac{\sigma_j}{\sigma_i}\right) + a_2\left(\frac{\sigma_j}{\sigma_i}\right)^2 \tag{10}$$

Values for a_0, a_1, and a_2 are given by Pirog (1998) for different particles and solids volume fractions based on the results of his settling experiments.

Kinetic Theory for a Bimodal Particle Mixture

In order to describe solid-phase stresses in the framework of the two-fluid model for dense gas-solids flows typically concepts from kinetic theory are employed. The kinetic theory for granular materials has been developed by Jenkins and Savage (1983), Lun et al. (1984), and others, analogous to the kinetic theory of gases (Chapman and Cowling, 1970), accounting for the inelastic nature of particle-particle collisions. This theory has been used by many researchers to successfully describe both dense and dilute dry particulate flows, as well as dense and dilute fluidized particulate flows. Almost all work to date has considered monodisperse particulate systems. However, Jenkins and Mancini (1987) have developed kinetic theory for a mixture of bimodal disks and a mixture of bimodal spheres assuming a Maxwellian velocity distribution of the disks or spheres. Lopez de Haro et al. (1983) have developed kinetic theory for a gas consisting of a mixture of multiple components, employing a revised Enskog method (Van Beijeren and Ernst, 1973). Using the approach of Lopez de Haro et al. (1983) as a basis, Jenkins and Mancini (1989), Zamankhan (1995), and Arnarson and Willits (1998) developed kinetic theory for a binary particle mixture of spheres involving perturbations to the Maxwellian velocity distribution. These latter theories, with modifications outlined below, are used in this work to describe the solid-phase stress and fluctuating velocities of the bimodal particle mix.

We consider a mixture of smooth, nearly elastic spheres of two different species A and B. These spheres have mass m_i, number density n_i, radius σ_i, and velocity c_i, where i is either species A or B. The mass density ρ_i is given by the product of m_i and n_i. The number density n and the mass density ρ of the mixture are given by the sum of the corresponding densities of the two constituents. The mean velocity of each species is denoted by $u_i \equiv \langle c_i \rangle$. The mass average velocity of the mixture can be written as

$$u_s = \frac{1}{\rho}(\rho_A u_A + \rho_B u_B) \tag{11}$$

The peculiar velocity of each species is defined as: $C_i \equiv c_i - u_s$. The diffusion velocity $\boldsymbol{v}_i$, which is absent from the kinetic theory for monodisperse mixture of particles, is defined as

$$\boldsymbol{v}_i \equiv \langle C_i \rangle = \langle c_i - u_s \rangle \tag{12}$$

It then follows that

$$\rho_A \boldsymbol{v}_A + \rho_B \boldsymbol{v}_B = 0 \tag{13}$$

The granular temperature is related to the peculiar velocity and, unlike the monosized particle theory, also to the mass of the individual particle specie

$$T_i = \frac{1}{3} m_i \langle C_i^2 \rangle \tag{14}$$

The mixture temperature can be written as $T = 1/n(n_A T_A + n_B T_B)$. The mixture balance of granular energy is

$$\frac{3}{2} n\left[\frac{\partial T}{\partial t} + \nabla\cdot(T u_s)\right] - \frac{3}{2} T \nabla\cdot(n_A \boldsymbol{v}_A + n_B \boldsymbol{v}_B) = -\nabla\cdot q - \bar{\bar{P}}_s : \nabla u_s + \sum_{k=A,B}(F_i + \rho_i g)\cdot(\eta_A \boldsymbol{v}_A + n_B \boldsymbol{v}B) - \gamma \tag{15}$$

where q is the mixture energy flux, $\bar{\bar{P}}_s$ is the total solids stress tensor of the mixture, F_i is the total drag force acting on species i, and γ is the rate of granular energy dissipation. The first term on the lefthand side denotes the time dependency of the mixture granular energy, the second term is the convection of the mixture granular energy, and the third term denotes the convection of mixture granular energy due to the relative species movement. On the righthand side, the first term denotes the diffusion of the mixture granular energy along the gradients in the mixture granular temperature, the second term is the creation of a mixture granular energy due to shear in the particle phase, the third term denotes the creation or dissipation of mixture granular energy due to external forces, and the last term is the dissipation of granular energy due to inelastic particle-particle collisions.

The mixture energy flux is defined as

$$q = \sum_{i=A,B}\left(\frac{1}{2}\langle \rho_i C_i C_i^2 \rangle + \sum_{k=A,B} q_{ik}\right) \tag{16}$$

The first term on the righthand side is a transport or kinetic contribution to the mixture energy flux, and the second term q_{ik} is a collisional contribution.

Similarly, the kinetic and collisional contributions to the solid-phase stress tensor are given as

$$\bar{\bar{P}}_{s,\text{kinetic}+\text{collision}} = \sum_{i=A,B}\left(\langle \rho_i C_i C_i\rangle + \sum_{k=A,B}\bar{\bar{P}}_{ik}\right) \quad (17)$$

where the first term represents the kinetic or transport contribution to the pressure tensor and the second part P_{ik} the collisional contribution. Using the revised Enskog theory, the equations for the pressure tensor and the energy flux can be expressed in terms of particle and flow parameters as (Jenkins and Mancini, 1989)

$$\langle \rho_i C_i C_i\rangle = n_i T\bar{\bar{I}} - n_i T b_{i0}\left(\bar{\bar{D}} - \frac{1}{3}\nabla u_s \bar{\bar{I}}\right) \quad (18)$$

$$\bar{\bar{P}}_{ik} = \frac{2}{3}\pi\sigma_{ik}^3 n_i n_k T\bar{\bar{I}} - \frac{8}{15} n_i n_k \pi\sigma_{ik}^3 g_{ik} T \times\left[b_{i0} + M_{ki} + \sqrt{\frac{2m_i m_k}{m_{ik}\pi T}}\,\sigma_{ik}\right]\cdot\left[\bar{\bar{D}} - \frac{1}{3}\nabla u_s \bar{\bar{I}}\right] \quad (19)$$

and

$$\frac{1}{2}\langle \rho_i C_i C_i^2\rangle = \frac{5}{4} n_i a_{i1}\sqrt{\frac{2T}{m_i}}\,\nabla T + \frac{5}{2} n_i\sqrt{\frac{T^3}{2m_i}}\,(nt_{i0}d_i + a_{i0}\nabla(\ln T)) \quad (20)$$

$$q_{ik} = 2\sqrt{\frac{2T}{m_i}}\, n_i n_k \sigma_{ik}^3 \pi g_{ik} M_{ik} M_{ki}\left[a_{i1} - \frac{2}{3}\sigma_{ik}\sqrt{\frac{1}{\pi M_{ki}}}\right]\nabla T - \sqrt{\frac{T^3}{2}}\,\frac{2}{3} n_i n_k \pi\sigma_{ik}^3 g_{ik} \cdot\left[\sqrt{\frac{1}{m_i}}\,(nt_{i0}d_i + a_{i0}\nabla\ln T)(M_{ik} - M_{ki}) + \sqrt{\frac{1}{m_k}}\,(nt_{k0}d_k + a_{k0}\nabla\ln T)\right] \quad (21)$$

where $\sigma_{ik} \equiv \sigma_i + \sigma_k$, $m_{ik} \equiv m_i + m_k$, and $M_{ik} \equiv m_i/m_{ik}$. For the coefficient b_{i0}, Jenkins and Mancini (1989) give for $i \neq k$

$$b_{i0} = 5\frac{b_i\left(n_i + \frac{2}{5}K_{ii} + \frac{4}{5}K_{ik}M_{ki}\right) + \frac{32}{3}\sqrt{\pi M_{ik}M_{ki}/2m_{ik}}\,\sigma_{ik}^2\left(n_k + \frac{2}{5}K_{kk} + \frac{4}{5}K_{ik}M_{ik}\right)}{g_{ik}n_i n_k\sqrt{T}\left[b_i b_k - \frac{512}{9}\sigma_{ik}^4\pi(M_{ik}M_{ik}/m_{ik})\right]} \quad (22)$$

$$b_i = 40\sigma_{ik}^2\sqrt{\frac{\pi M_{ik}M_{ki}}{2m_{ik}}}\left(\frac{2}{3} + \frac{2m_i}{5m_k}\right) + 8\sigma_{kk}^2\frac{n_k g_{kk}}{n_i g_{ik}}\sqrt{\frac{\pi}{m_k}} \quad (23)$$

where $K_{ik} \equiv 2/3\pi n_i n_k g_{ik}\sigma_{ik}^3$. For the coefficients a_{i0} and t_{i0}, there has been some confusion in the literature. Arnarson and Willits (1998) claim that Jenkins and Mancini (1989), Zamankhan (1997), and Hsiau and Hunt (1996) have developed incorrect expressions for these coefficients.

Moreover, Kincaid et al. (1987) have investigated the convergence of the orders of the Enskog approximation and found that the first-order Enskog approximation is not accurate, even for small differences in particle size and/or mass. Therefore, Arnarson and Willits (1998) calculate the necessary coefficients correctly and up to the second order. With $i \neq k$ their results are

$$a_{i0} = \frac{1}{2\rho}\sqrt{m_{ik}m_k}\,n_k\left(M_{ki}^{3/2}a_{i1} - M_{ik}^{3/2}a_{k1}\right) \quad (24)$$

$$a_{i1} = -\frac{15}{8\sqrt{\pi}\,n_i n_k g_{ik}\sigma_{ik}^2\sqrt{M_{ki}}}\left(\frac{\alpha_i n_i K_i + 13M_{ik}M_{ki}n_k K_k}{\alpha_i\alpha_k - 169M_{ik}^2M_{ki}^2}\right) \quad (25)$$

$$\alpha_i = 15M_{ki}^2 + 8M_{ik}M_{ki} + 6M_{ik}^2 + 2\sqrt{2}\,\frac{n_k g_{kk}\sigma_{kk}^2}{n_i g_{ik}\sigma_{ik}^2\sqrt{M_{ik}}} \quad (26)$$

$$t_{i0} = \frac{1}{2\rho}\sqrt{m_{ik}m_k}\,n_k\left(M_{ki}^{3/2}t_{i1} + M_{ik}^{3/2}t_{k1}\right) + \frac{3m_k}{8\sqrt{\pi}\,\rho n_i g_{ik}\sigma_{ik}^2\sqrt{M_{ki}}} \quad (27)$$

$$t_{i1} = \frac{3\sqrt{M_{ki}}}{8\sqrt{\pi}\,n_i n_k g_{ik}\sigma_{ik}^2}\left(\frac{\alpha_i - 13M_{ik}^2}{\alpha_i\alpha_k - 169M_{ik}^2M_{ki}^2}\right) \quad (28)$$

$$K_i = 1 + \frac{2}{5}\pi n_i g_{ii}\sigma_{ii}^3 + \frac{8}{5}M_{ik}M_{ki}\pi n_k g_{ik}\sigma_{ik}^3 \quad (29)$$

Because Jenkins and Mancini (1989) and Arnarson and Willits (1998) have only used bimodal kinetic theory to study the case of steady homogeneous shear, contributions to the total solids stress tensor linear in $\nabla\cdot u_s$ were not considered. When this term does play a role, the solids stress must be extended with a contribution incorporating the solids bulk viscosity. The bulk viscosity contribution can be expressed as (Bird et al., 1960)

$$\bar{\bar{P}}_{s,\text{bulk}} = \left(\lambda - \frac{2}{3}\mu\right)tr\left(\bar{\bar{D}}\right)\bar{\bar{I}} \quad (30)$$

where λ is the solids bulk viscosity and μ is the solids shear viscosity, which can be determined from Eqs. 19 and 18 by considering the terms linear in $\bar{\bar{D}}$. Following the derivation

for a binary mixture of gas molecules by Lopez de Haro and Cohen (1984), an equation for the bulk viscosity of elastic spheres can be derived

$$\lambda = \frac{2}{3} \sum_{i=A,B} \sum_{k=A,B} K_{ik} \sigma_{ik} \sqrt{\frac{2Tm_i m_k}{\pi m_{ik}}} \tag{31}$$

For nearly elastic particles, the perturbation on the Maxwellian velocity distribution can be employed to derive an expression for the total rate of energy dissipation. Jenkins and Mancini (1989) present the rate of energy dissipation in the lowest Enskog approximation. In the second-order Enskog approximation, it can be written as

$$\gamma = \sum_{i=A,B} \sum_{k=A,B} 2 g_{ik} \sigma_{ik}^2 n_i n_k \frac{m_k}{m_{ik}} \left(1 - e_{ik}^2\right) \sqrt{\frac{2\pi m_{ik} T^3}{m_i m_k}} \tag{32}$$

where e_{ik} is the coefficient of restitution for a collision of particle species i with particle species k. For the diffusion velocity of each specie, Jenkins and Mancini (1989) give

$$\boldsymbol{v}_i = -\sqrt{\frac{T}{2m_i}} \left(n t_{i0} \boldsymbol{d}_i + a_{i0} \nabla \ln T \right) \tag{33}$$

dependent on the diffusion force

$$\boldsymbol{d}_i = -\frac{\rho_i}{n\rho T} \left[\nabla P + \rho_k \left(\frac{F_i + \rho_i g}{m_i} - \frac{F_k + \rho_k g}{m_k} \right) \right] + \frac{1}{n} \left(n_i + 2 M_{ik} K_{ik} + K_{ii} \right) \nabla \ln T + \frac{n_i}{nT} \left(\frac{\partial \mu_i}{\partial n_k} \nabla n_k + \frac{\partial \mu_i}{\partial n_i} \nabla n_i \right) \tag{34}$$

Using the thermodynamic relationships (Reed and Gubbins, 1973)

$$P = -\left(\frac{\partial A}{\partial V} \right)_{T, N_k} \qquad \mu_i = \left(\frac{\partial A}{\partial N_k} \right)_{T, N_{k \neq i}}$$

and by using the dependency of P and μ_i on T, it can be shown that

$$\boldsymbol{d}_A = -\boldsymbol{d}_B \tag{35}$$

Because the chemical potential μ_i is only dependent upon T, n_i, and n_k

$$\nabla \mu_i = \frac{\partial \mu_i}{\partial n_k} \nabla n_k + \frac{\partial \mu_i}{\partial n_i} \nabla n_i + \frac{\partial \mu_i}{\partial T} \nabla T \tag{36}$$

The latter equation can be used to replace the derivatives in n_i and n_k in Eq. 34, and rewrite Eq. 34 in terms of derivatives depending upon the location only.

To date, all authors investigating binary particle mixtures use the radial distribution function of Mansoori et al. (1971)

$$g_{ik} = \frac{1}{1-\epsilon_s} + \frac{3\sigma_i \sigma_k}{\sigma_i + \sigma_k} \frac{\xi_2}{(1-\epsilon_s)^2} + 2 \left(\frac{\sigma_i \sigma_k}{\sigma_i + \sigma_k} \right)^2 \frac{\xi_2^2}{(1-\epsilon_s)^3} \tag{37}$$

where $\xi_p = 4\pi (n_A \sigma_A^p + n_B \sigma_B^p)/3$, and thus $\epsilon_s \equiv \xi_3$. This expression, however, does not tend to infinity when the total solids volume fraction ϵ_s approaches the maximum packing of spheres. Therefore, we propose a similar radial distribution function which has the correct limit for the solids volume fraction when approaching the maximum packing limit for a bimodal mixture of spheres

$$g_{ik} = \frac{1}{1 - \frac{\epsilon_s}{\epsilon_{s,\max}}} + \frac{3\sigma_i \sigma_k}{\sigma_i + \sigma_k} \frac{\xi_2}{\left(1 - \frac{\epsilon_s}{\epsilon_{s,\max}}\right)^2} + 2 \left(\frac{\sigma_i \sigma_k}{\sigma_i + \sigma_k} \right)^2 \frac{\xi_2^2}{\left(1 - \frac{\epsilon_s}{\epsilon_{s,\max}}\right)^3} \tag{38}$$

where $\epsilon_{s,\max}$ is the maximum solids volume fraction. The two radial distribution functions are compared in Figure 1. At high solids volume fraction, which often occurs in fluidized beds, the difference in radial distribution functions is large.

The chemical potential is a function of the radial distribution function and for a binary gaseous mixture (Reed and

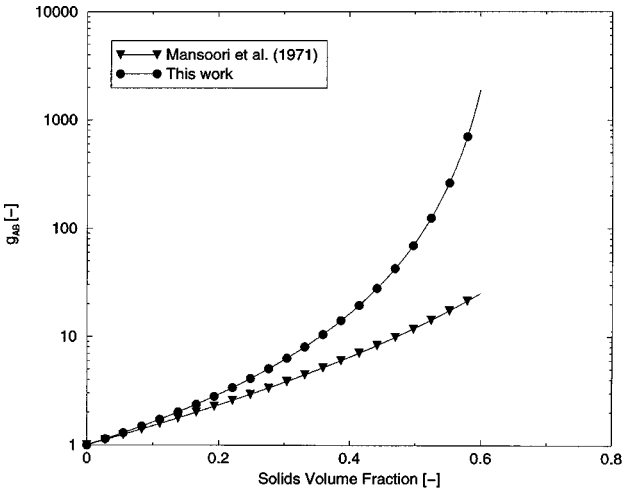

Figure 1. Radial distribution function of Mansoori et al. (1971) compared to the radial distribution function proposed in this work, for a 50/50 mix with $\sigma_A = 250$ μm and $\sigma_B = 100$ μm.

Gubbins, 1973)

$$\mu_i = kT \ln \frac{\rho_i \Lambda}{q_i^{\text{int}}} - \frac{2}{3}\pi kT \times \left(\frac{\partial}{\partial N_i} \left[\sum_{\alpha = A,B} \sum_{\beta = A,B} N_\alpha N_\beta \sigma_{\alpha\beta}^3 \int_\infty^V \frac{1}{V^2} g_{\alpha\beta}\, dV \right] \right)_{T,V,N_{k \neq i}} \tag{39}$$

where N_A and N_B are the total number of particles of each species, and thus $n_A = N_A/V$. Equation 39 has been solved with the new radial distribution function given in Eq. 38 using Mathematica (Wolfram, 1988), and the result is given in Appendix A. Shauly et al. (1988) use a semi-empirical model to predict the increase in the maximum solids volume fraction with different compositions of the binary mixture

$$\frac{\epsilon_{s,\max}}{\epsilon_{s,\max,\text{mono}}} = \left[1 + \frac{3}{2}|b|^{3/2} \left(\frac{\epsilon_{s,A}}{\epsilon_s} \right)^{3/2} \left(\frac{\epsilon_{s,B}}{\epsilon_s} \right) \right] \tag{40}$$

with $b = (\sigma_A - \sigma_B)/(\sigma_A + \sigma_B)$ and $\epsilon_{s,\max,\text{mono}}$ is the maximum solids volume fraction in the case of a monodisperse particle mixture equal to 0.65. Figure 2 shows an example of the variation of $\epsilon_{s,\max}$ as a function of mixture composition.

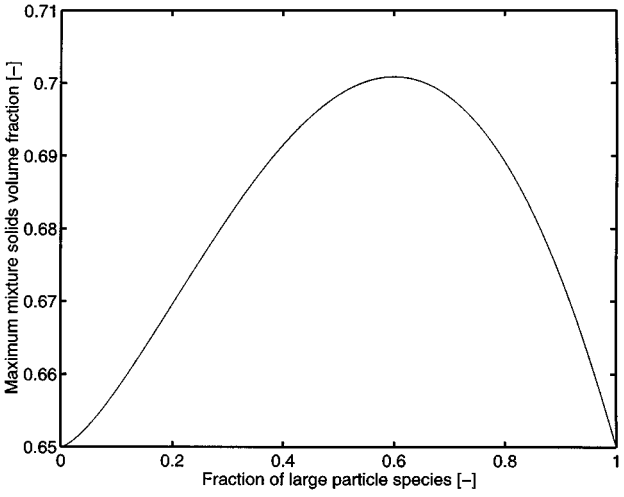

Figure 2. Maximum solids volume fraction, $\epsilon_{s,\max}$ of a mixture with $\sigma_A = 250$ μm and $\sigma_B = 100$ μm as a function of mixture composition.

Frictional Stress

In regions with very high solids volume fractions, as frequently present in fluidized beds, sustained contacts between particles occur. These frictional stresses must be accounted for in the description of the total solids-phase stress. The frictional stress is added to the kinetic and collisional contributions to the stress given by kinetic theory when the solid volume fraction exceeds some kick-in value $\epsilon_{s,\min}$. The frictional stress is in a Newtonian form (Johnson et al., 1990) and is added to the total stress tensor when $\epsilon_s > \epsilon_{s,\min}$, and the frictional stress is described by

$$\bar{\bar{P}}_{s,\text{friction}} = \begin{cases} P_f \bar{\bar{I}} + \mu_f \left(\nabla \boldsymbol{v} + (\nabla \boldsymbol{v})^T \right) & \text{if } \epsilon_s > \epsilon_{s,\min} \\ 0 & \text{if } \epsilon_s \leq \epsilon_{s,\min} \end{cases} \tag{41}$$

where P_f represents the normal frictional stress and μ_f represents the frictional shear viscosity. For the normal frictional stress, the semi-empirical equation of Johnson and Jackson (1987) is employed

$$P_f = Fr \frac{(\epsilon_s - \epsilon_{s,\min})^q}{(\epsilon_{s,\max} - \epsilon_s)^p} \tag{42}$$

The values proposed by Johnson et al. (1990) for the empirical material constants are $Fr = 0.05$ Nm^{-2}, $q = 2$, and $p = 5$, for particles similar to those studied in this work. The frictional shear viscosity is related to the frictional normal stress by the linear law proposed by Coulomb (1776)

$$\mu_f = P_f \sin \phi \tag{43}$$

where ϕ represents the angle of internal friction. This frictional stress model assumes a monodisperse PSD and does not contribute to or initiate segregation.

Simulations

The CFD model as just described is used to simulate two-dimensional gas-solid fluidized beds at different superficial gas velocities and with different particle weights and sizes. In summary, the solution of the eight primary variables u_s, u_g, n_a, n_b, T, and P, is achieved by solving the nine Eqs. 2, 3, 4, 5, 13, and 15.

Simulations of fluidized beds have been performed with a bimodal PSD for two cases of particles and mixture properties, as given in Table 1. In Case 1, we have also performed a

Table 1. Physical Properties of the Binary and Monodisperse Particle Systems

Particles	Dia. (2σ) (μm)	Dens. (kg·m^{-3})	U_{mf} (m/s)	Terminal Vel. (m/s)	Avg. Mass Fract.	Avg. Vol. Fract.
			Bimodal Mixture: Case 1			
Glass beads	500	2,640	0.19	20	0.5	0.21
Glass beads	200	2,640	0.04	3.2	0.5	0.21
			Monodisperse mixture with same Sauter mean diameter			
Glass beads	485	2,640	0.18	19	1.0	0.42
			Bimodal Mixture: Case 2			
Polystyrene	500	1,150	0.09	8.2	0.30	0.21
Glass beads	200	2,640	0.04	3.2	0.70	0.21

Table 2. System Properties and Computational Parameters

Parameter	Description	Value
ρ_g (kg/m^3)	Gas density	1.28
μ_g (Pa·s)	Gas viscosity	1.7×10^{-5}
e	Coefficient of restitution	0.9
e_w	Wall coefficient of restitution	0.9
a_0	Empirical constant Eq. 10	11.28
a_1	Empirical constant Eq. 10	−9.69
a_2	Empirical constant Eq. 10	1.49
ϵ_{max}	Maximum monodisperse solids volume fraction	0.65
ϕ	Angle of internal friction	28
D_T (m)	Inner column diameter	0.15
H_t (m)	Column height	0.3
H_{mf} (m)	Height at minimum fluidization	0.16
$\epsilon_{s,mf}$ (m)	solids volume fraction at minimum fluidization	0.42
Δx (m)	x mesh spacing	1.00×10^{-2}
Δy (m)	y mesh spacing	1.00×10^{-2}
Δt (s)	Timestep	1.00×10^{-5}

simulation of a fluidized bed with a monodisperse PSD exhibiting the same Sauter mean diameter as the bimodal PSD. The employed fluidization and computational parameters are given in Table 2. The calculation of the minimum fluidization velocities is based upon the empirical correlation of Wen and Yu (1966). Due to the coarseness of the particles, the minimum fluidization velocity is equal to the minimum bubbling velocity.

The simulations in this work were carried out with the commercial CFD code CFX 4.2 from AEA Technology, Harwell, U.K. The equations for the solids-phase stress for the bimodal particle mixture, the solids mixture temperature, the drag on the particle mixture, and the diffusion velocities were implemented into this code. For solving the differential equations, the higher-order total variation diminishing (TVD) scheme Superbee is employed. This scheme is a modification of the higher-order upwind scheme. The SIMPLE algorithm is used to correct the pressure from the gas phase velocities (Patankar, 1980). The gas phase is assumed to be compressible and the calculated pressure is used to determine the gas-phase density.

Initially, the bottom part of the fluidized bed is filled with a random mixture of two particles at rest with a uniform solids volume fraction. In Case 1, the mass fraction is set 0.5 for both the large and small particles. In Case 2, the solids volume fraction is set equal; the mass fractions are not equal because the density of each species is different.

Limiting case validation runs were performed with the CFD code describing the bimodal particle mixture by setting the volume fraction of one particle species to 10^{-5} and the other to a realistic value; hence, the hydrodynamics of the flow should be completely determined by the particle species with the large volume fraction. The results in terms of bed expansion and bubble size gave results at two simulated superficial gas velocities equal to the CFD code employing the granular kinetic theory for a monodisperse particle mixture, as employed by Van Wachem et al. (1998, 2000). The computational effort for a run with the CFD code describing the bimodal particle mixture, however, is increased by one order of magnitude over a run involving the monodisperse particle mixture. Because of the magnitude of the required computational effort, each simulation has been performed up to 14 s of real time. One simulation takes almost four weeks of computational time on a 166 Mhz IBM RS 6000 computer. Hence, on these short time-scales, it was impossible to obtain good statistics on bubble behavior or on the dynamics of the pressure fluctuations.

Boundary Conditions

All the simulations were carried out in a two-dimensional Cartesian space in which front and back wall effects are neglected. The left and right walls of the fluidized bed are treated as no-slip boundaries for the gas phase and free-slip boundaries for the particle mixture. The boundary condition for the mixture temperature follows the equation of Johnson and Jackson (1987) for a monosized particle configuration, but is corrected for the difference in definition of the mixture temperature (Eq. 14)

$$n\cdot q=\frac{\pi\rho\epsilon_s\sqrt{\dfrac{3Tn}{\rho\epsilon_s}}}{6\epsilon_{s,\max}\left[1-\left(\dfrac{\epsilon_s}{\epsilon_{s,\max}}\right)^{1/3}\right]}\left[\varphi'|u_{\text{slip}}|^2-\frac{3T_n}{2\rho\epsilon_s}\left(1-e_w^2\right)\right] \tag{44}$$

where φ' is the specularity coefficient. The first term represents the generation of mixture temperature due to particle slip at the wall, while the second term represents dissipation of fluctuating energy due to inelastic particle-wall collisions. Simulations performed with an adiabatic boundary condition at the wall ($\nabla T = 0$) show very similar results.

The boundary condition at the top of the free-board (fluid-phase outlet) is a pressure boundary; the pressure at this boundary is fixed to a reference value. Neumann boundary conditions are applied to the gas flow, requiring fully developed gas flow. The solids volume fraction is held constant to 10^{-6} at the outlet to ensure convergence and a meaningful finite valued solids velocity field in the free-board. In this way, the whole freeboard is filled with a very small number of particles, which does not influence the behavior of the fluidized bed.

At the bottom of the fluidized bed, Dirichlet boundary conditions are employed for the gas phase in which the superficial gas velocity is specified. The bottom is made impenetrable for the solids phase by setting the solids axial velocity to zero.

Results and Discussion

Bimodal mixture Case 1

Figure 3 shows a visual representation of the total solids volume fraction and the relative diffusion velocity of the larger species for bimodal mixture Case I. It can be clearly seen that the time-dependent segregation mainly occurs in and near voids, and that bubbles are the cause of this segregation behavior. The relative diffusion velocity is much larger in and near voids than in the dense particulate phase, because particles have space to ''vibrate'' and can move much more easily.

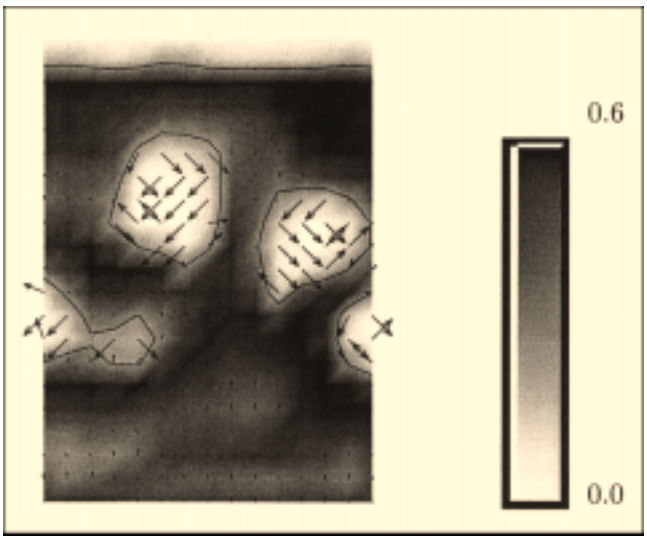

Figure 3. Total solids volume fraction indicating the bubbles and the bed surface with contour lines and indicating the relative velocity of the larger particles.

Figure 4 shows that the bed expansion is larger in the fluidized bed with a bimodal mixture than in the fluidized bed with a monodisperse mixture. This result is consistent with the results of De Groot (1967) and Grace and Sun (1991). The difference in bed expansion is mainly due to the upward diffusion of the smaller particle species. For the case presented in Figure 4, a layer of small particles dominates the mixtures top 25% of the bed.

Figure 5, which gives the variation in bed expansion as a function of the fluidization velocity, shows the difference in the bed expansion between the bimodal and the monodisperse case. The difference in the bed expansion between the bimodal and monodisperse cases with increasing gas velocity reaches a maximum and then begins to decrease as the particle mixing in the bimodal case improves, as well presented in Figure 6. The minimum fluidization velocity of the bimodal mixture determined from the simulation results is $U_{mf} = 0.14$ m/s, whereas the minimum fluidization velocity of the equivalent monodisperse mixture is $U_{mf} = 0.19$ m/s. This observation also agrees with the studies done by De Groot (1967) and Grace and Sun (1991). Part of the difference between the bed expansion behavior and the shift of the minimum fluidization velocity can be explained because the gravity force depends on a different type of averaging (see Eq. 9).

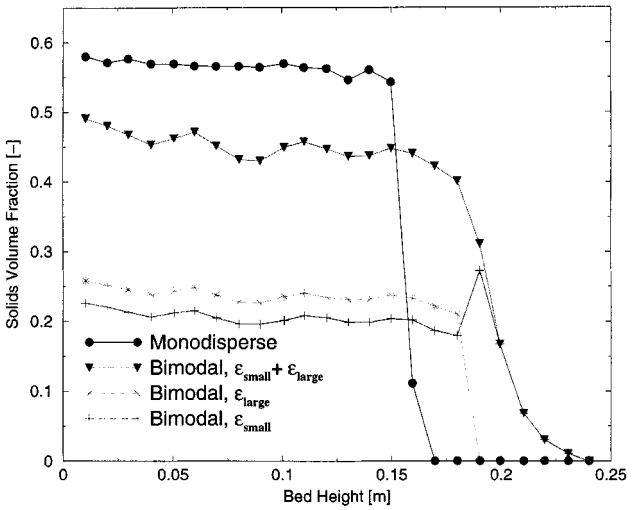

Figure 4. Strip-averaged solids volume fraction as a function of bed height for the bimodal mixture and the monodisperse mixture Case 1 (Table 1) at $U = 0.27$ m/s.

For the bimodal mixture, the total solids volume fraction and the solids volume fraction of the individual large and small particle species are shown.

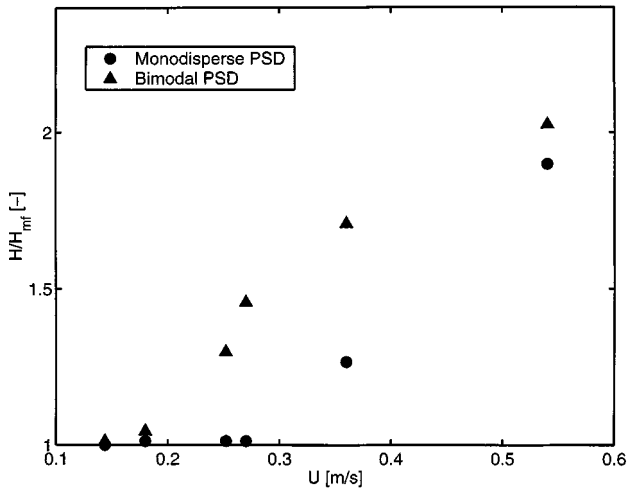

Figure 5. Predicted bed expansion as a function of superficial gas velocity for the bimodal particle mixture Case 1 (Table 1) compared with a monodisperse particle mixture.

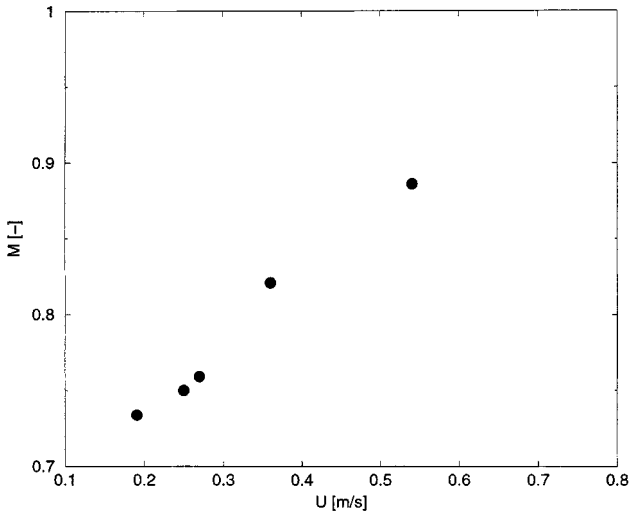

Figure 6. Predicted mixing index as a function of superficial gas velocity for the bimodal particle mixture Case 1 (Table 1).

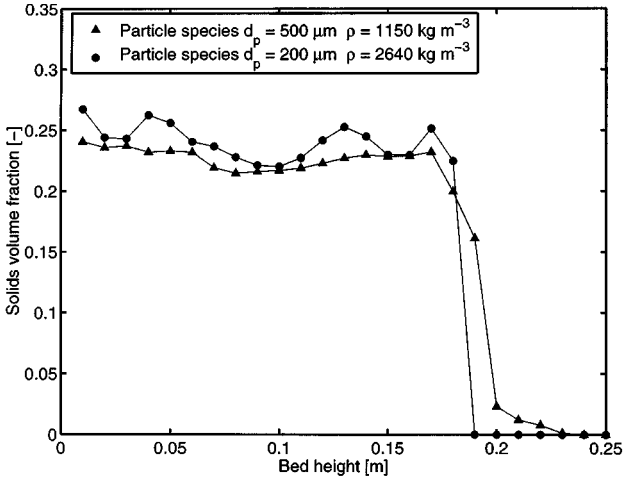

Figure 7. Strip- and 4 s time-averaged solids volume fraction of the bimodal mixture Case 2 fluidized bed at $U = 1.08$ m/s.

The lines are drawn to guide the eye.

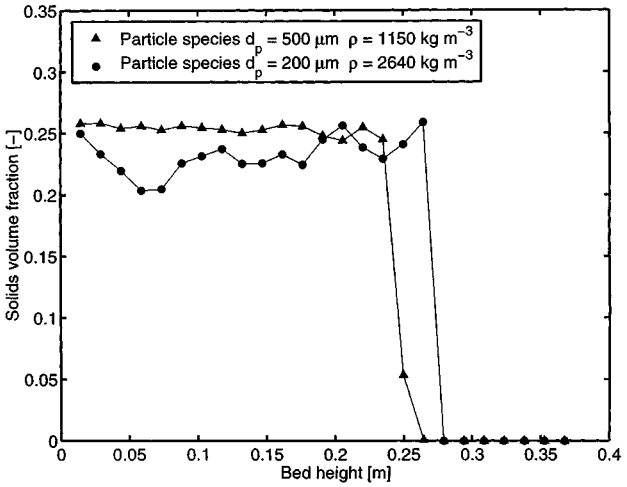

Figure 8. Strip- and 4 s time-averaged solids volume fraction of the bimodal mixture Case 2 fluidized bed at $U = 1.85$ m/s.

The lines are drawn to guide the eye.

Figure 6 shows the result of the computation of the mixing index based on the simulations of the bimodal mixture Case 1. The mixing index was determined by dividing the solids volume fraction of the large particles in the top 25% of the fluidized bed by the average solids volume fraction of the large particles in the entire bed. At velocities above the minimum fluidization velocity, the predicted mixing index increases with superficial gas velocity, conforming with the experiments and observations of Wu and Baeyens (1998). The thickness of the layer of finer species occurring in the top of the bed decreases with increasing superficial gas velocity and the top layer of particles in the fluidized bed is more well mixed.

Bimodal mixture Case 2

Two simulations were performed of a fluidized bed containing the bimodal particle mixture of different solid sizes and densities. Figure 7 shows the last four seconds of fourteen seconds *s* time-averaged solids volume fraction as a function of bed height with a fluidization velocity of $U = 1.08$ m/s. It is clearly seen that the larger, lighter particles segregate to the top of the fluidized bed and the smaller and heavier particles segregate downwards. Due to the short time averaging, the spread on the points is fairly large.

The results for a higher gas velocity, $U = 1.85$ m/s, shown in Figure 8, show the opposite segregation behavior. Due to the much larger granular temperature and granular temperature gradients, the diffusion force is directed in the opposite direction compared to the diffusion force at the lower gas velocity. Both averages were determined in the interval between 10 and 14 s of real time. Although these times are much too short to predict the final segregated state and a quantative comparison with the literature is therefore not possible, the trends shown are the same as reported by Rasul et al. (1999).

Rasul et al. (1999) gave empirical rules of thumb when inversion can take place, but from the kinetic theory of a binary mixture of particles, inversion can be easily explained. The diffusion force and diffusion velocity, described by Eqs. 33 and 34, are dependent on four quantities: the gradient in granular pressure, the gradient in granular temperature, the gradient in chemical potential, and the difference in drag and gravity force between one particle species and the other. In the case that Rasul et al. (1999) studied, the drag and gravity force difference between the small and heavy particles and the large and light particles is dominant at low gas velocity. At low gas velocity, both the gravity force and the upward drag force lead to a much smaller upward force for the small and heavy particles. Hence, the diffusion force and thus the diffusion velocity cause a downward movement of the small and heavy particles. When the gas velocity is increased, however, the gradients in granular temperature and granular pressure become dominant terms in the equations for the diffusion force and the diffusion velocity.

Conclusions

In this article we describe a CFD model for gas-fluidized beds containing a bimodal particle-size distribution. In the fluidized bed, the particle phase stress, associated with particle velocity fluctuations, is predicted by means of the granular kinetic theory for a binary mixture of smooth, nearly elastic spheres.

The employed CFD model correctly predicts the increased bed expansion compared to fluidized beds with a monodisperse particle-size distribution, as observed in experiments by de Groot (1967). Related to this, the minimum fluidization velocity is also significantly lowered in the simulations with a bimodal particle-size distribution, as experimentally observed by Grace and Sun (1991). The CFD model with a bimodal particle-size distribution is also able to show inversion, as observed by Rasul et al. (1999). The five physical effects derived from first principles causing inversion are presented, based upon the granular kinetic theory for a bimodal mixture.

Finally, it is noted that the calculation times for the bimodal mixture are extremely large, increased by an order of magnitude of a monodisperse simulation. Therefore, with current computational power, it is not possible to predict the behavior of fluidized beds containing a bimodal mixture over a time-scale of even a few seconds of fluidized beds with a realistic size in a timely fashion.

Acknowledgments

The investigations were supported (in part) by the Netherlands Foundation for Chemical Research (SON) with financial aid from the Netherlands Organization for Scientific Research (NWO). This support is largely acknowledged. B. G. M. van Wachem gratefully acknowledges the financial support of the Netherlands Organization for Scientific Research (NWO), the Stimulation fund for Internationalization (SIR), DelftChemTech, the Delft University Fund, and the Reactor Research Foundation (RR) for the expenses for visiting Purdue University.

Notation

A = free energy, $kg \cdot m^2 \cdot s^{-2}$
b = empirical constant
c = particle velocity, $m \cdot s^{-1}$
C = peculiar particle velocity, $m \cdot s^{-1}$
C_D = drag coefficient
d = particle diameter, m
d = diffusion force, m^{-7}
D_T = inner column diameter, m
$\overline{\overline{D}}$ = rate of strain tensor $= 1/2[\nabla u + (\nabla u)^T]$, s^{-1}
F = external force/drag force, N
Fr = empirical material constant, $N \cdot m^{-2}$
g = radial distribution function
g = gravitational constant, $m \cdot s^{-2}$
H = height in fluidized bed, m
m = particle mass, kg
M = mixing index
n = normal vector, m
n = number density, m^{-3}
p = empirical material constant
P = normal pressure, $N \cdot m^{-2}$
Re_p = particle Reynolds number
q = empirical material constant
q = mixture energy flux, $kg \cdot m^2 \cdot s^{-3}$
T = granular temperature, $kg \cdot m^2 \cdot s^{-2}$
u = average velocity, $m \cdot s^{-1}$
U = superficial gas velocity, $m \cdot s^{-1}$
$\boldsymbol{v}$ = diffusion velocity, $m \cdot s^{-1}$
V = volume of a particle, m^3
X = small species volume fraction

Greek letters

β = interphase drag constant, $kg \cdot m^{-3} \cdot s^{-1}$
γ = rate of granular energy dissipation, $kg \cdot m \cdot s^{-3}$
ϵ = volume fraction
ϕ = angle of internal friction
φ' = specularity coefficient
λ = bulk viscosity, $Pa \cdot s$
μ = shear viscosity, $Pa \cdot s$
μ_i = chemical potential
ρ = density
σ = particle radius, m
$\overline{\overline{\tau}}$ = viscous stress tensor, $N \cdot m^{-2}$

Subscripts

A = first particle species
B = second particle species
g = gas phase
i = ith particle species
k = kth particle species
ik = employ properties of species i and k
max or m = maximum
mf = at minimum fluidization
min = minimum; kick-in value
mono = monodisperse particle size distribution
s = solids mixture
slip = slip
w = wall

Literature Cited

Arnarson, B. O., and J. T. Willits, "Thermal Diffusion in Binary Mixtures of Smooth, Nearly Elastic Spheres with and without Gravity," *Phys. Fluids*, **10**, 1324 (1998).
Bird, R. B., W. E. Stewart, and E. N. Lightfoot, *Transport Phenomena*, Wiley, New York (1960).
Chapman, S., and T. G. Cowling, *The Mathematical Theory of Non-Uniform Gases*, Cambridge University Press, 3d ed. (1970).
Coulomb, C. A., "Essai sur une Application des Règles de Maximis et Minimis à Quelques Problèmes de Statique, Relatifs à l'Architecture," *Acad. R. Sci. Mém. Math., Phys. par Divers Savants*, **7**, 343 (1776).
de Groot, J. H., *Proc. Intern. Symp. Fluidization*, A. H. H. In Drinkenberg, ed., Netherlands University Press, Amsterdam, p. 348 (1967).
Grace, J. R., and G. Sun, "Influence of Particle Size Distribution on the Performance of Fluidized Bed Reactors," *Can. J. Chem. Eng.*, **69**, 1126 (1991).
Hsiau, S. S., and M. L. Hunt, "Granular Thermal Diffusion in Flows of Binary-Sized MIxtures," *Acta Mech.*, **114**, 121 (1996).
Jackson, R., "Locally Averaged Equations of Motion for a Mixture of Identical Spherical Particles and a Newtonian Fluid," *Chem. Eng. Sci.*, **52**, 2457 (1997).
Jenkins, J. T., and F. Mancini, "Balance Laws and Constitutive Relations for Plane Flows of a Dense, Binary Mixture of Smooth, Nearly Elastic Circular Disks," *J. Appl. Mech.*, **54**, 27 (1987).
Jenkins, J. T., and F. Mancini, "Kinetic Theory for Binary Mixtures of Smooth, Nearly Elastic Spheres," *Phys. Fluids A*, **1**, 2050 (1989).
Jenkins, J. T., and S. B. Savage, "A Theory for the Rapid Flow of Identical, Smooth, Nearly Elastic, Spherical Particles," *J. Fluid Mech.*, **130**, 187 (1983).
Johnson, P. C., and R. Jackson, "Frictional-Collisional Constitutive Relations for Granular Materials, with Application to Plane Shearing," *J. Fluid Mech.*, **176**, 67 (1987).
Johnson, P. C., P. Nott, and R. Jackson, "Frictional-Collisional Equations of Motion for Particulate Flows and Their Application to Chutes," *J. Fluid Mech.*, **210**, 501 (1990).
Kincaid, J. M., E. G. D. Cohen, and M. Lopez de Haro, "The Enskog Theory for Multicomponent Mixtures: IV. Thermal Diffusion," *J. Chem. Phys.*, **86**, 963 (1987).
Lopez de Haro, M., and E. G. D. Cohen, "The Enskog Theory for Multicomponent Mixtures: III. Transport Properties of Dense Binary Mixtures with One Tracer Component," *J. Chem. Phys.*, **80**, 408 (1984).
Lopez de Haro, M., E. G. D. Cohen, and J. M. Kincaid, "The Enskog Theory for Multicomponent Mixtures. I. Linear Transport Theory," *J. Chem. Phys.*, **78**, 2746 (1983).
Lun, C. K. K., S. B. Savage, D. J. Jefferey, and N. Chepurniy, "Kinetic Theories for Granular Flow: Inelastic Particles in Couette Flow and Slightly Inelastic Particles in a General Flowfield," *J. Fluid Mech.*, **140**, 223 (1984).
Mansoori, G. A., N. F. Carnahan, K. E. Starling, and T. W. Leland, Jr., "Equilibrium Thermodynamic Properties of the Mixture of Hard Spheres," *J. Chem. Phys.*, **54**, 1523 (1971).
Patankar, S. V., *Numerical Heat Transfer and Fluid Flow*, Hemisphere Publishing Corporation, Washington, DC (1980).
Pirog, T. W., "Dynamics of Destabilization of Flood Emulsions. Measurement and Simulation of Gravity Driven Particle Velocities in Polydisperse Dispersions," PhD Thesis, Purdue University (1998).
Rasul, M. G., V. Rudolph, and M. Carsky, "Segregation Potential in Binary Gas Fluidized Beds," *Powder Technol.*, **103**, 175 (1999).
Reed, T. M., and K. E. Gubbins, *Applied Statistical Mechanics*, McGraw-Hill, New York (1973).

Rowe, P. N., "Drag Forces in a Hydraulic Model of a Fluidized Bed: II," *Trans. Inst. Chem. Engs.*, **39**, 175 (1961).
Shauly, A., A. Wachs, and A. Nir, "Shear-Induced Particle Migration in a Polydisperse Concentrated Suspension," *J. Rheol.*, **42**, 1329 (1998).
van Beijeren, H., and M. H. Ernst, "The Modified Enskog Equation," *Physica*, **68**, 437 (1973).
van Wachem, B. G. M., J. C. Schouten, R. Krishna, and C. M. van den Bleek, "Eulerian Simulations of Bubbling Behaviour in Gas-Solid Fluidised Beds," *Comput. Chem. Eng.*, **22**, s299 (1998).
van Wachem, B. G. M., J. C. Schouten, R. Krishna, C. M. van den Bleek, and J. L. Sinclair, "Comparative Analysis of CFD Models of Dense Gas-Solid Systems," *AIChE J.*, in press (2001).
Wen, C. Y., and Y. H. Yu, "Mechanics of Fluidization," *Chem. Eng. Progr. Symp. Ser.*, **62**, 100 (1966).
Wolfram, S., *Mathematica*, Addison-Wesley Publishing (1988).
Wu, S. Y., and J. Baeyens, "Segregation by Size Difference in Gas Fluidized Beds," *Powder Technol.*, **98**, 139 (1998).
Zamankhan, P., "Kinetic Theory of Multicomponent Dense Mixtures of Slightly Inelastic Spherical Particles," *Phys. Rev. E*, **52**, 4877 (1995).
Zamankhan, P., Comment and Authors' Reply to "Granular Thermal Diffusion in Flows of Binary-Sized Mixtures," *Acta Mech.*, **123**, 235 (1997).

Appendix A

The chemical potential for the radial distribution coefficient is defined in Eq. 39. i indicates one particle species, and k the other ($i \neq k$). n_i is defined as N_i/V where N_i is the total number of particles for each specie. The meaning of the symbols can be found in the Notation section, and *max* has been abbreviated to m. The result for species i is

$$\mu_i = T\Bigg[\ln(n_i) - \frac{1}{\left(\sigma_i^3 n_i + n_k \sigma_k^3\right)^4} \cdot \Bigg\{ \frac{2\epsilon_m \sigma_i^2}{\left[4\pi\left(\sigma_i^3 n_i + n_k \sigma_k^3\right) - 3\epsilon_m\right]^3} \cdot \Big[4\pi\left(\sigma_i^3 n_i + n_k \sigma_k^3\right)\Big\{32\sigma_i\pi^2\left(\sigma_i^3 n_i + n_k \sigma_k^3\right)^4\left(\sigma_i^3 n_i^2 + n_k^2 \sigma_k^3\right) - 9\epsilon_m^4\left(\sigma_i^2 n_i + n_k \sigma_k^2\right)\left(\sigma_i^8 n_i^3 - \sigma_i^6 n_i^2 n_k \sigma_k^2 + 4\sigma_i^5 n_i^2 n_k \sigma_k^3 + \sigma_i^3 n_i n_k^2 \sigma_k^5 - 3\sigma_i n_k^3 \sigma_k^7 + 2n_k^3 \sigma_k^8\right) + 3\epsilon_m^3\left(\sigma_i^3 n_i + n_k \sigma_k^3\right)\Big[\sigma_i^7 n_i^3\left(9 + 10\sigma_i^3 n_i \pi\right) + \sigma_i^4 n_i^2 n_k\left(27 + 40\sigma_i^3 n_i \pi\right)\sigma_k^3 - \sigma_i^3 n_i n_k^2\left(9 + 10\sigma_i^3 n_i \pi\right)\sigma_k^4 + 2\sigma_i^2 n_i n_k^2\left(9 + 25\sigma_i^3 n_i \pi\right)\sigma_k^5 - 18\sigma_i n_k^3 \sigma_k^6 - n_k^3\left(20\sigma_i^3 n_i \pi - 9\right)\sigma_k^7 + 20\sigma_i^2 n_i n_k^3 \pi \sigma_k^8 - 30\sigma_i n_k^4 \pi \sigma_k^9 + 20 n_k^4 \pi \sigma_k^{10}\Big] - 48\epsilon_m \pi\left(\sigma_i^3 n_i + n_k \sigma_k^3\right)^3\Big[\sigma_i^5 n_i^2 n_k \pi \sigma_k^2 + 2\sigma_i^3 n_i n_k^2 \pi \sigma_k^4 - 2\sigma_i^2 n_i n_k^2 \pi \sigma_k^5 - n_k^3 \pi \sigma_k^7 + \sigma_i^4 n_i^2\left(1 - 3n_k \pi \sigma_k^3\right) + \sigma_i n_k^2 \sigma_k^3\left(1 + 3n_k \pi \sigma_k^3\right)\Big] - 2\epsilon_m^2\left(\sigma_i^3 n_i + n_k \sigma_k^3\right)^2\Big(4\sigma_i^{10} n_i^4 \pi^2 - 16\sigma_i^8 n_i^3 n_k \pi^2 \sigma_k^2 - 20\sigma_i^6 n_i^2 n_k^2 \pi^2 \sigma_k^4 + 24\sigma_i^2 n_i n_k^2 \pi \sigma_k^5\left(3 + n_k \pi \sigma_k^3\right) + 12 n_k^3 \pi \sigma_k^7\left(3 + 2n_k \pi \sigma_k^3\right) + 6\sigma_i^7 n_i^3 \pi\left(3 + 8n_k \pi \sigma_k^3\right) + 9\sigma_i^4 n_i^2\left(12 n_k \pi \sigma_k^3 - 1\right) - 2\sigma_i^3 n_i n_k^2 \pi \sigma_k^4\left(27 + 20n_k \pi \sigma_k^3\right) + 2\sigma_i^5 n_i^2 n_k \pi \sigma_k^2\left(26 n_k \pi \sigma_k^3 - 9\right) - \sigma_i n_k^2 \sigma_k^3\left[9 + 2n_k \pi \sigma_k^3\left(45 + 22 n_k \pi \sigma_k^3\right)\right]\Big\}\Big] + \Big[(2 - \epsilon_m)(\epsilon_m - 1)\sigma_i^{10} n_i^4 - 2\sigma_i^7 n_i^2\{2(\epsilon_m - 2)(\epsilon_m - 1)n_i - n_k\} n_k \sigma_k^3 + (\epsilon_m - 3)\epsilon_m \sigma_i^6 n_i^2 n_k^2 \sigma_k^4 - \epsilon_m(5\epsilon_m - 6)\sigma_i^5 n_i^2 n_k^2 \sigma_k^5 + \sigma_i^4 n_i n_k^2\left[(9\epsilon_m - 10)n_i + 4n_k - 6\epsilon_m n_k\right]\sigma_k^6 + 2\epsilon_m^2 \sigma_i^3 n_i n_k^3 \sigma_k^7 - 2(\epsilon_m - 3)\epsilon_m \sigma_i^2 n_i n_k^3 \sigma_k^8 + \sigma_i n_k^3\left[(2 + 3(\epsilon_m - 2)\epsilon_m\right]n_k - 4n_i)\sigma_k^9 + (3 - 2\epsilon_m)\epsilon_m n_k^4 \sigma_k^{10}\Big]\ln(3) - \Big[(\epsilon_m - 2)(\epsilon_m - 1)\sigma_i^{10} n_i^4 + 2\sigma_i^7 n_i^2\left[2(\epsilon_m - 2)(\epsilon_m - 1)n_i - n_k\right]n_k \sigma_k^3 - (\epsilon_m - 3)\epsilon_m \sigma_i^6 n_i^2 n_k^2 \sigma_k^4 + \epsilon_m(5\epsilon_m - 6)\sigma_i^5 n_i^2 n_k^2 \sigma_k^5 - \sigma_i^4 n_i n_k^2\left[(9\epsilon_m - 10)n_i + 4n_k - 6\epsilon_m n_k\right]\sigma_k^6 - 2\epsilon_m^2 \sigma_i^3 n_i n_k^3 \sigma_k^7 + 2(\epsilon_m - 3)\epsilon_m \sigma_i^2 n_i n_k^3 \sigma_k^8 + \sigma_i n_k^3\{4n_i - \left[2 + 3(\epsilon_m - 2)\epsilon_m\right]n_k\}\sigma_k^9 + \epsilon_m(2\epsilon_m - 3)n_k^4 \sigma_k^{10}\Big](\ln(\epsilon_m) - \ln\left[3\epsilon_m - 4\pi\left(\sigma_i^3 n_i + n_k \sigma_k^3\right)\right]\Bigg]$$

Manuscript received Apr. 19, 2000, and revision received Oct. 9, 2000.